

## REVIEW

[View Article Online](#)  
[View Journal](#) | [View Issue](#)

Cite this: *Mater. Adv.*, 2022,  
3, 7445

Received 18th December 2021,  
Accepted 24th July 2022

DOI: 10.1039/d1ma01199e

[rsc.li/materials-advances](http://rsc.li/materials-advances)

# MXenes: promising 2D materials for wound dressing applications – a perspective review

Vaishnavi Hada,<sup>a</sup> Deeksha Malvi,<sup>a</sup> Medha Mili,<sup>†a</sup> Manal M Khan,<sup>b</sup> Gaurav Chaturvedi,<sup>b</sup> SAR Hashmi,<sup>†a</sup> AK Srivastava<sup>†a</sup> and Sarika Verma<sup>†a</sup>

Two-dimensional (2D) materials have been studied extensively for the past 15 years, sparking a new wave of research on well-known 2D materials. Due to their specific configuration and noteworthy physicochemical features, intensive, multifaceted research attempts have been focused on the medical and clinical applications of 2D materials. In this context, 2D MXenes, a new class of ultra-thin atomic nanosheet materials produced from MAX phase ceramics, are gaining popularity as inorganic nanosystems, especially for biomedical applications. The 2D MXenes can meet the stringent biomedical standards due to their high conductivity, hydrophilicity, and other interesting physicochemical properties. Based on these characteristics, 2D MXenes have been used in wound dressing management and there are many studies on the development of nanofibers and nanosheets. Herein, we present an overview of MXenes, and their synthesis using various processes and properties. The review further focuses on the mechanism and importance of MXenes for wound dressing applications. Additionally, we summarize the toxicity and bio-safety issues of MXene-based materials. In the last section, we present the conclusions, challenges and future outlook.

## 1. Introduction

Over the last few years, incredible potential and many intriguing opportunities have resulted in the development of commercial adaptable nano-materials for disease and patient-specific treatment.<sup>1,2</sup> Among the various nanostructures, two-dimensional (2D) nanomaterials have become a research focus in the world of nanoscience. 2D nanomaterials have shown potential for wide application ranging from well-developed

<sup>a</sup> Council of Scientific and Industrial Research-Advanced Materials and Processes Research Institute, Bhopal (M.P.), 462026, India.

E-mail: [drsarikaverma20@gmail.com](mailto:drsarikaverma20@gmail.com), [sarika.verma@ampri.res.in](mailto:sarika.verma@ampri.res.in)

<sup>b</sup> All India Institute of Medical Sciences (AIIMS), Bhopal, (M.P.), 462026, India

<sup>†</sup> Academy of Council Scientific and Industrial Research-Advanced Materials and Processes Research Institute (AMPRI), Hoshangabad Road, Bhopal (M.P.), 462026, India.



**Vaishnavi Hada**

*Ms Vaishnavi Hada is a Project Associate at the Council of Scientific and Industrial Research-Advanced Materials and Process Research Institute (CSIR-AMPRI). She is a postgraduate and her research is focused on developing smart and functional biomaterials such as shape-memory polymer composites for sutures and wound healing applications, nano-biomaterials, advanced radiation shielding materials, biomass utilization, and antimicrobial materials useful for versatile applications.*



**Deeksha Malvi**

*Ms Deeksha Malvi is a post-graduate at the Council of Scientific and Industrial Research-Advanced Materials and Process Research Institute (CSIR-AMPRI). Her area of interest is biochemistry research. She mainly works on developing advanced materials via various chemical processes for a broad application. She is working on chitosan and lignin-based antimicrobial gels for wound healing applications, and is also interested in the scaling up of methods using alternative approaches.*

power storage to burgeoning medicinal chemistry. In the case of 2D materials, MXenes are emerging materials, which were discovered in 2011 by etching an MAX phase by chemical treatment.<sup>3</sup> MXenes have the general formula of  $M_{n+1}X_nT_x$ , where M represents an early transition metal such as Ti. Meanwhile, X represents nitrogen and/or carbon, T represents a surface functional group such as O, OH, and F, x represents the number of functional groups, and n stands for a positive integer between 1 and 4.<sup>4</sup> MXenes are a family of 2D crystalline solids with a substantial available diameter range. Further, their nanoscale density is distinguished by their endpoints or surface elements, which give them well-defined attributes.<sup>5</sup> Owing to this, MXene research has progressed, with scientists attempting to comprehend their features and uses.<sup>6</sup>

Due to their unique tensile characteristics, physio-chemical characteristics (e.g., photonic, catalytic, magnetic, and electronic properties) and numerous other exciting features, MXenes have attracted significant interest from researcher.<sup>7</sup> Because of the partially occupied d-shells of their transition metal atoms and their peculiar coordination with neighbouring atoms, most MXenes are metallic.<sup>8</sup> Also, it should be highlighted that the surface modification of MXenes can enhance their electronic attributes. Moreover, because most MXenes are metallic, their electronic properties are primarily influenced by their M atoms. Surface modification can also have an impact on the magnetization of MXenes.<sup>9</sup> This can result in a surface-functionalized MXene with weaker magnetization, which is caused by the transition metal element that has unpaired surface electrons.<sup>10</sup>



**Medha Mili**

*Mrs Medha Mili is working as a Scientist at the Council of Scientific And Industrial Research–Advanced Materials and Process Research Institute (CSIR–AMPRI). Her research areas mainly include polymer composites/nanocomposites, polymer processing, advanced bamboo-based polymeric composites for structural applications, advanced lignocellulosic materials based composites, and shape-memory polymer composites.*



**Manal M Khan**

*Dr Manal Mohd Khan is presently an Additional Professor and Head, the Department of Burns and Plastic Surgery, All India Institute of Medical Sciences, Bhopal, Madhya Pradesh. He did his MS (Surgery) and MCh (Plastic & Reconstructive Surgery) at the prestigious J. N. M. C., Aligarh Muslim University, and Fellowship in Aesthetic & Laser Surgery. His clinical and research interests include micro-vascular surgery, onco-reconstruction, brachial plexus injury surgery, cranio-maxillo-facial surgery, and management of various burns and post-traumatic wounds. He has published multiple papers in national and international journals and contributed various book chapters.*



**Gaurav Chaturvedi**

*Dr Gaurav Chaturvedi is an Associate Professor in the Dept. of Burns & Plastic Surgery at All India Institute of Medical Sciences, Bhopal, Madhya Pradesh. He brings his clinical experience to his role at AIIMS, Bhopal, after training for over six years at Christian Medical College, Vellore, one of the premier Institutes in India. His clinical and research interest includes managing patients with brachial plexus injury, onco-*

*reconstruction, and managing wounds and their coverage, especially in burns and trauma patients, with the help of microvascular surgery. He has published multiple research papers in the International and National Journal on Wounds Management.*



**SAR Hashmi**

*Dr SAR Hashmi is the Chief Scientist at the Council of Scientific and Industrial Research–Advanced Materials and Process Research Institute (CSIR–AMPRI). He specializes in the development of polymer composites such as bamboo-based polymeric composites and shape-memory polymers. He also works on the processing and rheology of polymers, blends and composites, design and development of components, products and experiments.*



Furthermore, magnetic MXenes with half-metallic functionalities have been studied. One spin channel is semi-conducting, while the other is metallic, giving rise to completely spin-polarized electrons at the Fermi level.<sup>11</sup> Besides, the surface terminations of MXenes play a significant role in their mechanical characteristics. The proportion of atomic layers of MXenes, depending on their chemical formula, is another variable that affects their mechanical characteristics. MXene-polymer composites have been shown to have significantly greater compression strength and tensile properties, durability, and functionality than pure MXenes.<sup>12</sup> It has been reported that the optical properties of MXenes, such as their refractive index, reflectivity, absorption, and transmittance, are essential in various applications. Some investigations on the effect of the surface functionalization of MXenes on their optical characteristics have been reported.<sup>13</sup> Moreover, the visible and UV light absorption of MXenes is the keystone for their optoelectronic, photo-voltaic and photocatalytic properties, which are influenced by the presence of functional groups.<sup>14</sup>

In the recent clinical advancement, bioengineering and nanobiotechnology have sparked the development of various innovative synthetic nanomaterials. These innovative nanomaterials give alternative theranostic (therapeutic and diagnostic) methods as possible solutions to counter various diseases through synergistic treatment and multimodal imaging, particularly in cancer therapies.<sup>15–25</sup> Their multiple features, such as porous structure and fascinating physio-chemical natures, enable them to meet the stringent requirements of theranostic nanomedicine, including drug administration, laser treatment, radiology, biosensors, and even wound healing.<sup>19,26–33</sup> Bio-sensing, antimicrobial materials, biomedical imaging, photo-thermal therapy nanomedicine, cancer detection and therapy are a few applications besides wound dressing.<sup>34</sup>

A wound is an interruption in the cohesiveness of the epithelial lining of the skin or mucosa caused by physical or thermal impairment.<sup>35</sup> Wound curing is a dynamic and

complicated tissue proliferation and growth procedure, which occurs in four stages, as follows: (i) agglomeration and haemostasis process (instantly after damage); (ii) inflammation process (soon after tissue damage), after which swelling occurs; (iii) proliferation process, in which new skin cells and vasculature are developed; and (iv) maturation process, in which new skin cells are remodelled.<sup>36</sup> In the 4 healthcare sectors, MXene-based materials have become the most promising and effective advanced materials in wound dressing applications. Wound dressings containing microbicidal compounds have emerged as excellent solutions for reducing wound infection, thus increasing the speed of the recovery process.<sup>37</sup> MXene-based materials have demonstrated strong bactericidal and wound-healing potential, paving the way for the development of new wound healing dressings and antimicrobial techniques.<sup>38</sup>

The present review highlights the synthesis of MXene-based materials using various processes and their properties. Further, we focus on the mechanism and importance of MXenes for wound dressing applications. Additionally, we summarize the toxicity and bio-safety issues associated with MXene-based materials. In the last section, we present the conclusions, challenges and future outlook.

## 2. Synthesis and general properties of MXene-based materials

### 2.1 Synthesis of MXenes

MXene is the name given to a group of transition metal nitrides, carbides and carbonitrides assembled by molecular deformation of a MAX phase, which is 3D ternary (or quaternary) composition.<sup>39</sup> The MAX phase is an MXene precursor with the stoichiometric ratio of  $M_{n+1}AX_n$ , where “M” is a d-block transition metal, “A” is a group 13 or 14 component (e.g., Si, Sn, Ge and Al), and “X” is nitrogen, carbon, or both.<sup>40</sup> The layers “M” and “A” are agglomerated in these portions, which have a



**AK Srivastava**

*Dr A. K. Srivastava is the Director of the Council of Scientific and Industrial Research-Advanced Materials and Processes Research Institute (CSIR-AMPRI). His prolific research applied to understanding the nucleation-growth mechanisms, phase transformations, microstructures and defects of various materials in the form of bulk and fascinating nanoscale is outstanding and known by peers worldwide. He has contributed significantly to multiple projects*

*in the area of advanced materials about (i) biomaterials, (ii) rapidly solidified metallic systems, (iii) nanostructures, (iv) polymer composites, (v) solar energy, (vi) thermoelectrics, (viii) magnetic, (viii) waste to wealth, and (ix) safety, health & environment.*



**Sarika Verma**

*Dr Sarika Verma is currently working as the Principal Scientist at Council Of Scientific and Industrial Research-Advanced Materials and Processes Research Institute (CSIR-AMPRI). Her areas of interdisciplinary research primarily include the design and development of advanced materials including materials for health care applications, radiation shielding materials, biomedical and energy materials, and polymeric composites such as bamboo-based*

*polymeric composites and shape-memory polymers via novel techniques useful for a wide range of applications. She is also the recipient of various awards and fellowships.*





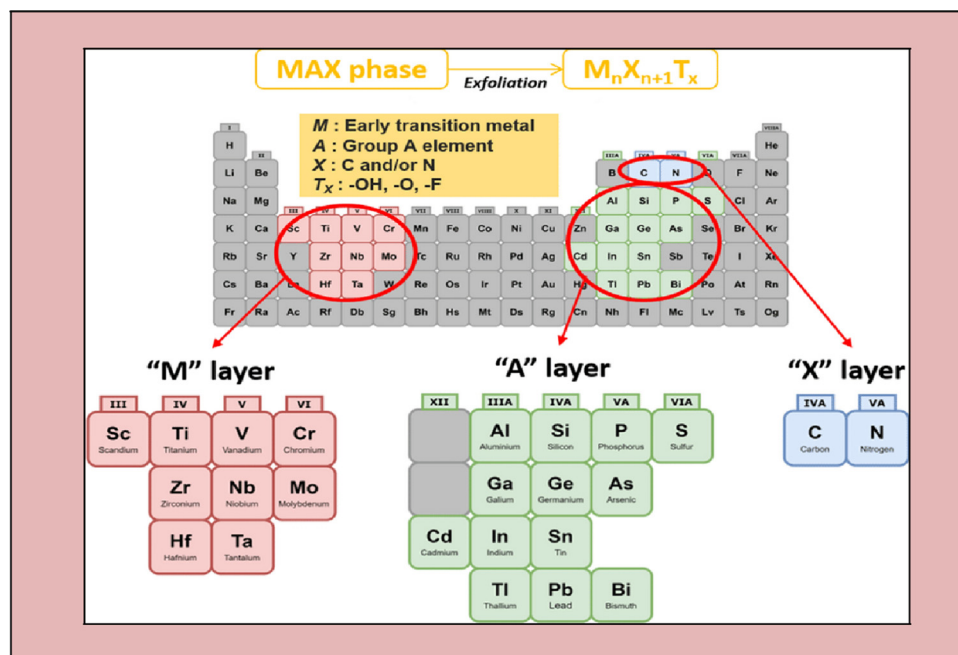


Fig. 1 Composition of the general elements of MXenes and MAX phases, where M is an early transition metal, A is a group A element, X is N and/or C, and T<sub>x</sub> is a surface functional group (adapted from ref. 46 under Creative Commons Attribution 4.0).

hexagonal shape (space group  $P63/mmc$ ). The "X" atoms occupy the octahedral positions created by the "M" atoms.<sup>41–45</sup> Fig. 1 illustrates the general elemental composition of MXenes.

The bond stress of M–X and M–A is the fundamental MAX phase difference. Alternatively, M–A is weakly bonded and more fragile than the M–X bonds.<sup>47–49</sup> The central concept for the synthesis of MXenes is removing the weakly linked A atoms layers to create carbides, nitrides, or both,<sup>50</sup> which is the critical stage in their synthesis.<sup>51</sup> This series of 2D metal nitrides and carbides created is termed MXenes due to the deletion of the A atom layer from the MAX phase.<sup>52</sup> Because the layer-to-layer bonding in the MAX phase is substantially weaker than the intra-layer bonding, wet chemical etching of the atomic layers in a multilayered MAX phase is the most popular method for the preparation of MXenes. The MAX phase is initially immersed in acid, which dissolves the bonding between the transition metal and the A element.<sup>53</sup>

After synthesizing the MAX phase, the primary step is to etch the 3D MAX phase, such as  $\text{Ti}_3\text{AlC}_2$ , with a strong etchant, commonly hydrofluoride (HF).<sup>54</sup>

In comparison to M–X bonds, M–A bonds are more fragile, and hence the specific etching of the M–A bonds can be achievable.<sup>55</sup> Given that F ions bond tightly to the A-element, etching the A-element from the typical MAX phase demands a higher accumulation of fluoride ions (F) (or Al).<sup>55</sup> Furthermore, HF processing of the MAX phase produces surface terminations with –O, –F, and –OH molecules, as represented in Fig. 2.<sup>56</sup>

The first etchant employed was hydrofluoric acid (HF), which is highly hazardous to the environment.<sup>58–60</sup> This problem was solved using various processes in which the use of HF is not required. Consequently, the necessity for multiple etchants emerged. In 2014, a better combination of HCl (hydrochloric acid)

and LiF (lithium fluoride) was introduced.<sup>61</sup> The HF acid etching approach boosted the hydrophilic functional groups such as F, OH and O on the surface of MXenes, which define their augmented hydrophilic properties, resulting in enhanced biocompatibility.<sup>62</sup>

(i) **Chemical vapour deposition.** Taking methane ( $\text{CH}_4$ ) as the source of carbon (C) and copper (Cu) foil above molybdenum (Mo) foil as the substrate, Xu *et al.* established a CVD (chemical vapour deposition) technique to create MXenes in 2015<sup>63</sup> at a temperature of more than 1085 °C. The breakdown of chemicals on the plane of the substrate throughout the CVD process resulted in the formation of material layers from the vapour phase. The Cu foil melted because of the elevated temperature, formed an Mo–Cu alloy. Upon interacting with the carbon atoms created *via* the combustion of methane, the Mo-atoms diffused into the surface of the Cu liquid, generating  $\text{Mo}_2\text{C}$ -crystals. Despite its MXene-like structure, the created substance was a 2D transition metal carbide with a more extensive size than the previously developed nanosheets of up to 10 mm. Researchers were able to alter the diameter by adjusting the methane content. Once the MXene-like substance was exposed to air for several months, it was devoid of flaws, and its super-conductivity remained unchanged.

(ii) **Urea glass route.** Using urea glass, Ma *et al.* (2015)<sup>64</sup> produced  $\text{Mo}_2\text{C}$  and  $\text{Mo}_2\text{N}$  MXenes from the metal precursor  $\text{MoCl}_5$ . They introduced ethanol to the precursor, which reacted, resulting in the formation of Mo-orthoesters. Subsequently, solid urea was added to the mixture and agitated until it was completely dissolved. After that, the gel-like product was calcined at 800 °C in an  $\text{N}_2$  gas atmosphere. They obtained silvery black particles and performed XRD (X-ray diffraction) analysis on the samples and found no other crystalline side phases, such as  $\text{MoOx}$ , indicating that the powder was pure.

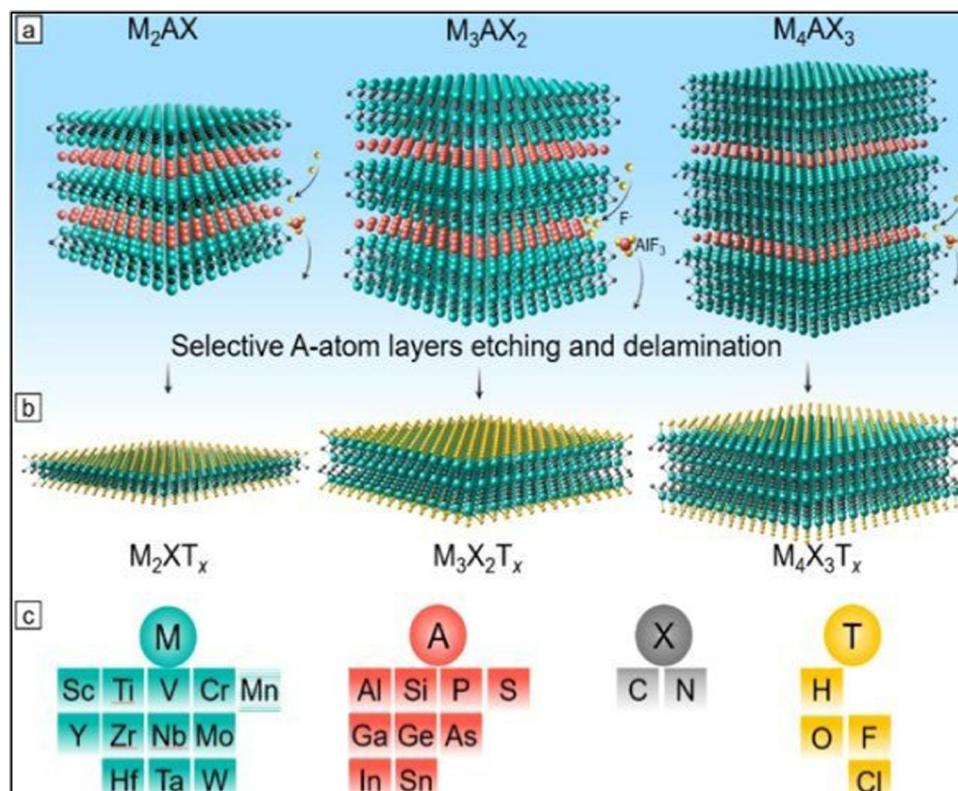


Fig. 2 Precursors and synthesis of MXenes. (a) Three types of mono-M MAX phases:  $M_2AX$ ,  $M_3AX_2$ , and  $M_4AX_3$  and the selective etching process of the group A layers (red atoms). (b) Formation of MXene after selective etching and the formation of surface terminations (yellow atoms) labeled as T. (c) Feasible elements for M, A, X, and T in MAX and MXene phases (adapted with permission from ref. 57 Copyright©2021).

(iii) **Hydrothermal synthesis in an aqueous solution of NaOH.** In 2018, Li *et al.*<sup>65</sup> published a method for the preparation of  $Ti_3C_2T_x$ MXene from the  $Ti_3AlC_2$  MAX phase using NaOH (sodium hydroxide). In this method, the  $(OH-OH-)$  hydroxide anions damaged the aluminium (Al) layers, causing the Al-atoms

to be oxidized. The generated aluminium hydroxides, *i.e.*,  $Al(OH)_4^-$  were subsequently dispersed in the alkali, with the exposed Ti (titanium) atoms being exchanged with O or OH. This procedure allows new aluminium hydroxides in the matrix of Ti layers, and therefore they react with  $OH-OH-$  again. The MXenes

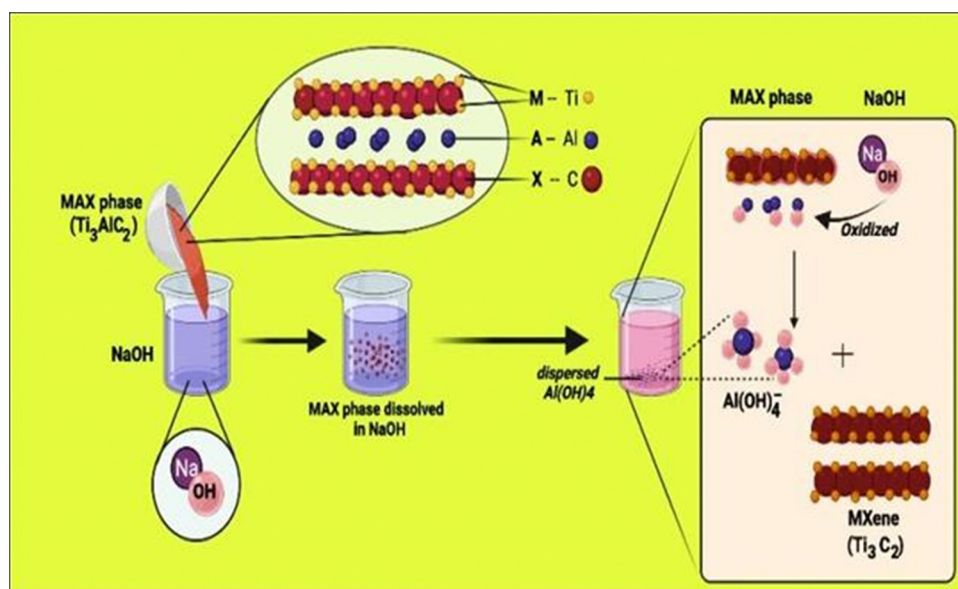


Fig. 3 Formation of MXene via hydrothermal synthesis using  $Ti_3AlC_2$  (MAX phase) and NaOH solution.

**Table 1** Various methods employing etchants to obtain MXenes

S. no.	Method	Etchants	Temperature	Ref.
1	—	NaBF <sub>4</sub> , HCl	180 °C	6
2	Acid with and without fluorine	HF	Room temp. 55 °C	54
3	—	HCl + LiF	35–55 °C	61
4	Hydrothermal	NaOH	270 °C	65
5	Electrochemical	NH <sub>4</sub> Cl/TMAOH	Room temp.	66
6	—	HCl	Room temp.	67
7	Molten salts	LiF + NaF + KF	550 °C	68
8	—	NH <sub>4</sub> HF <sub>2</sub>	Room temp.	70
9	Lewis acid	ZnCl <sub>2</sub>	550 °C	71

acquired by this hydrothermal process had more O and OH terminations than that obtained by HF etching, significantly improving their supercapacitor efficiency. Fig. 3 represents the formation of MXenes *via* hydrothermal synthesis using Ti<sub>3</sub>AlC<sub>2</sub> (MAX phase) and NaOH solution.

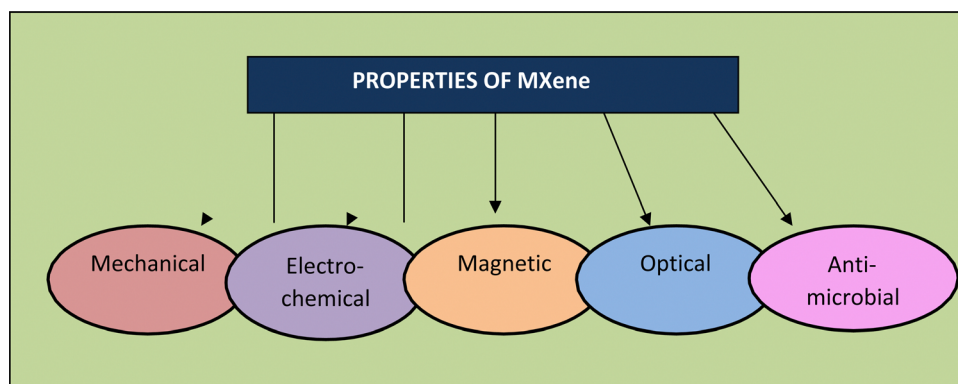
(iv) **Electrical synthesis at room temperature.** Yang *et al.* (2018)<sup>66</sup> reported the first electrochemical technique for debonding Ti<sub>3</sub>C<sub>2</sub> in a dual electrolyte solution. Bulk Ti<sub>3</sub>AlC<sub>2</sub> was used as the anode and cathode in a two-electrode arrangement; however, only the anode was etched, resulting in Ti<sub>3</sub>C<sub>2</sub>T<sub>x</sub>.<sup>67</sup> They employed a pH > 9 mixture of 1 M NH<sub>4</sub>Cl and 0.2 M tetramethylammonium hydroxide (TMAOH) to permit the electrolyte atoms to permeate a certain depth in the anode. The core anode was progressively deformed using a low voltage of +5 V. To make individual sheets of Ti<sub>3</sub>C<sub>2</sub>T<sub>x</sub>, the residue of Ti<sub>3</sub>C<sub>2</sub>T<sub>x</sub> was crushed and put into 25% w/w TMAOH. The electrical conductivity of the generated MXenes was comparable to that synthesized using HCl or HF/LiF. However, the electrochemical approach is more attractive given that in the overall etching productivity, almost 60% of the material mass can be converted into Ti<sub>3</sub>C<sub>2</sub>T<sub>x</sub>.<sup>61</sup>

(v) **Molten salt etching.** The approach of etching molten salt was first employed on MXenes in 2016. Urbankowski *et al.*<sup>68</sup> heated Ti<sub>4</sub>AlN<sub>3</sub> powder in a 1 : 1 mass ratio with fluoride salt for about 550 °C for 30 min. They discovered five distinct fluoride phases comprising aluminium, but no Ti-comprising fluorides, proving the etching sensitivity. They utilized dilute sulfuric acid (H<sub>2</sub>SO<sub>4</sub>) to disseminate the Al-containing fluorides, and the etching residues were eliminated by rinsing with deionized water, centrifugation, and decanting. The powder

was further combined with tetrabutylammonium hydroxide to break down the layered Ti<sub>4</sub>N<sub>3</sub>T<sub>x</sub> MXene (TBAOH). The small unlayered Ti<sub>4</sub>N<sub>3</sub>T<sub>x</sub> flakes (T = OH, FT = OH, and F) were recovered after processing. Table 1 describes the different etching methods used to obtain MXenes.<sup>69</sup> Some of the etchants include HF, HCl + LiF, NH<sub>4</sub>HF<sub>2</sub>, NH<sub>4</sub>Cl/TMAOH, LiF + NaF + KF, ZnCl<sub>2</sub>, NaBF<sub>4</sub>, HCl, and NaOH.

## 2.1 General properties of MXenes

MXenes possess valuable essential characteristics (as shown in Fig. 4), including structural, electrical, optical, and biological properties.<sup>72</sup> These characteristics make them suitable for extensive applications, with the latest being in healthcare. High specific surface area, availability of hydrophilic groups, high molecular weights (for certain transition metals), and magnetization properties are all hallmarks of MXenes.<sup>73–75</sup> The latest innovations in biology and electronics using MXenes have realized a new era of technology in the field of bio-electronics for healthcare assistance and theranostics, medical observation, and wearable devices.<sup>76–78</sup> Bioelectronic devices are invented for the safest association with human body tissues, offering a prototype-changing chance for monitoring brain activity, cardiac health, and muscle function. They can also assist human-machine interactions, such as myo-electric control of advanced prostheses<sup>79,80</sup> and brain-computer interfaces (BCIs).<sup>81</sup> Active bio-electronic components can also be applied by the smart approach depending on the electrical stimulation of excitable circuits for treating neurological diseases,<sup>82,83</sup> heart

**Fig. 4** Properties of MXenes.



arrhythmias<sup>84</sup> and inflammatory disorders<sup>85,86</sup> and used for rehabilitation therapies. The functional groups of MXenes also enhance their rigidity and elasticity, which are applicable for thin-film production in bio-electronic equipment.<sup>87</sup>

**(i) Mechanical properties.** The mechanical characteristics of MXenes can vary significantly, depending on their surface terminations. Bai *et al.* (2016)<sup>88</sup> discovered that the Ti atoms and O terminations interacted more strongly in Ti<sub>2</sub>C and Ti<sub>3</sub>C<sub>2</sub> than in OH or F-terminated MXenes. Furthermore, O-terminated MXenes have very high strength and stiffness, signifying that the bond stability of Ti–O is superior compared to Ti–F and Ti–OH.

Magnuson *et al.* (2018)<sup>89</sup> also discovered that the surface groups diminish C bonds by removing their energy. They found that the Ti–C bond is more robust in Ti<sub>2</sub>CT<sub>x</sub> than Ti<sub>3</sub>C<sub>2</sub>T<sub>x</sub>, which they believe may alter the elasticity of these materials. Scientists also proposed that modifying the binding strength can help improve the flexibility of MXenes. Furthermore, because of their higher structural rigidity, Zha *et al.* (2016)<sup>90</sup> indicated that O-terminated MXenes should be the primary candidates as structural materials, supercapacitors, and other purposes.

In theory, Ti<sub>2</sub>CO<sub>2</sub>-based composite materials can withstand considerable strain under uniaxial and deformation tension. Regarding the strain endurance of MXenes, Chakraborty *et al.* (2017)<sup>91</sup> demonstrated the doping of Ti<sub>2</sub>CO<sub>2</sub> with boron (B), where boron replaces the carbon atoms, which could withstand excessive strain (almost 100%) compared to the undoped MXene. This is because of the weak bond between Ti–B and Ti–C bond. Furthermore, Yorulmaz *et al.* (2016)<sup>92</sup> discovered that MXenes stiffen as the density of M, *i.e.*, transition metal, increases for carbides, although this finding was not observed for nitrides.

**(ii) Electronic properties.** The strong electronic conductivity of MXenes is their most vital electronic feature. The majority of uncoated MXenes and those with surface terminations have metallic characteristics. Although Ti<sub>3</sub>C<sub>2</sub>T<sub>x</sub> was the first identified, the longest investigated, and the most active MXene, an endeavour has been undertaken to boost the metallic conductivity of MXenes in recent years.<sup>93</sup> The focus is producing new M<sub>n+1</sub>X<sub>n</sub>M<sub>n+1</sub>X<sub>n</sub> compounds with regulated surface terminations to increase their resistivity. Unfortunately, there is no scientific confirmation for the research done in this area.<sup>94</sup> The formation of cation or organic–molecule complexes is an alternative way to influence the resistivity of MXenes. An almost absolute scale can enhance the susceptibility of devices to layered substances.<sup>95,96</sup>

Zhang *et al.* (2018)<sup>97</sup> found that OH-terminated MXenes had free electron energies outside the particle surface and parallel to the surface. They form clusters in areas with the most significant positive charge, providing nearly perfect electron transport routes. At the Fermi level, the transition metal has a reduced density of states (DOS) because of the electron transport from a transition metal to the electronegative surface terminations.<sup>98,99</sup> No MXene semiconductors have been investigated to date, even though most are anticipated to have a band gap for all surface terminations.<sup>100</sup>

**(iii) Magnetic properties.** The most prevalent MXenes, together with Ti<sub>3</sub>C<sub>2</sub>, are non-magnetic; however, various magnetic frameworks have been revealed. For example, Dong *et al.* (2017)<sup>101</sup> reported that Ti<sub>2</sub>MnC<sub>2</sub>T<sub>x</sub> MXenes in the ground state are ferromagnetic. Ti<sub>2</sub>MnC<sub>2</sub>T<sub>x</sub> is associated with the new family of double ordered-transition-metal MXenes,<sup>102,103</sup> which have a transition metal of one or two layers that joins with the other layers. Sun *et al.* (2018)<sup>104</sup> investigated a central layer consisting of double-transition-metal MXenes with Ti atoms. It has also demonstrated that various terminations and cation arrangements result in magnetic characteristics and attributes distinct from the previously known single transition metal carbides.<sup>105,106</sup>

Previously, Zhu *et al.* (2015)<sup>107</sup> discovered a conceptual in-plane lattice fixed standard for Nb<sub>2</sub>C, which agrees with the experimental one, and demonstrated that the thermodynamically favourable place for Li sorbent was situated on the upper end of the MXene. Bandyopadhyay *et al.*,<sup>108</sup> explored the process of node deformation in MXenes in 2018. They discovered that a few deficient MXenes exhibit magnetism due to the delocalized electrons in their rotation-torn d-orbitals. Consequently, they proposed that inherent defects could be used to alter the magnetization of MXenes.

**(iv) Optical property.** Various intriguing optical properties of MXenes have been documented in recent years, including plasmonic behaviour, optical transparency, and photothermal conversion efficiency. The potential of MXenes to interact with light in several ways has had a massive effect on the scientific community.<sup>109</sup> Specifically, the surface terminations play a significant role in determining their optical properties. Halim *et al.*, 2019<sup>110</sup> studied Ti<sub>2</sub>CT<sub>x</sub> and Nb<sub>2</sub>CT<sub>x</sub> films and demonstrated that changing the transition metal is a novel method of controlling the reflectivity of MXenes. They discovered that the permeability of the Nb-based films increased, as shown by their infrared spectra. These actions varied greatly for the correlating MAX sequence Nb<sub>2</sub>AlC, which was not detected for the titanium-based films. Halim *et al.*<sup>55</sup> recommended that the discrepancy in optical characteristics was due to the electron pairs of the transition metals (titanium in group 4 of the periodic table, while Nb is in group 5), their bond formation with carbon atoms and surface termination.

Li *et al.* (2017)<sup>65</sup> demonstrated that in comparison with carbon nanotubes (CNTs), MXenes accumulate more light. Furthermore, Jiang *et al.* (2018)<sup>111</sup> investigated the optical nonlinearity of Ti<sub>3</sub>C<sub>2</sub>T<sub>x</sub> using oscillation sources with different wavelengths (1800 nm, 1550 nm, 1064 nm, and 800 nm). They discovered that the permeability reaction was two orders of magnitude greater than several other mechanisms, but the refractive index of graphene was similar. Finally, for Ti<sub>2</sub>N, Ti<sub>3</sub>N<sub>2</sub>, Ti<sub>2</sub>C, and Ti<sub>3</sub>C<sub>2</sub>, their reflectivity reached 100%, indicating these materials can transmit electromagnetic waves.<sup>112</sup>

**(v) Antimicrobial property.** Before MXenes, nanomaterials based on graphene were used in biomedical applications to produce reactive oxygen species (ROS) and directly interact with the cell wall of microbes.<sup>1,113–116</sup> The first Ti<sub>3</sub>C<sub>2</sub>MXene nanoparticle solution demanded a significant inhibition dose of 200 g to provide favorable suppression.<sup>117,118</sup> Nevertheless, the



modification of  $\text{Ti}_3\text{C}_2$  with PVDF (polyvinylidene fluoride) significantly improved its antimicrobial activity.<sup>117</sup> One study proposed that due to the unique characteristics of MXene nanostructures such as their sharp edges and compact size, they can pierce the bacterial cell membrane, resulting in the release of bacterial DNA and ultimately bacterial dispersion.<sup>119</sup> The only report on the anti-fungal properties of MXene was investigated using  $\text{Ti}_3\text{C}_2$  MXene against *T. reesei* (*Trichoderma reesei*).<sup>120</sup> The influence of delaminated MXene ( $\text{d-Ti}_3\text{C}_2$ ) inhibited the development of hyphae in *T. reesei*, which yielded similar findings to the anti-fungal medicine amphotericin-B. Because of their sharp lamellar periphery, MXene nanosheets may also impede sporulation. Consequently, this study demonstrated that  $\text{Ti}_3\text{C}_2$ MXene may destabilize the fungal life cycle and indicated the tremendous capacity of MXenes as convincing anti-fungal agents. Because of their significant microbicidal actions, the chemistry of MXenes enables future applications in previously unexplored areas such as coating materials for medical catheters, masks, and gloves.<sup>46</sup>

### 3. Why and how are MXene-based materials helpful for wound dressing applications?

Wounds can occur due to severe trauma, diabetes, and burns as a disorder profoundly influencing human health and causing tough challenges in the field of healthcare.<sup>121–125</sup> Although several remedies for wound healing, such as drug therapies,<sup>126</sup> skin grafting,<sup>127</sup> and cellular treatment,<sup>128</sup> are used in medical care, they have some restrictions that limit their therapeutic effects. Because of their distinctive attributes, MXenes have intrigued many researchers in the biomedical field,<sup>38,123,129,130</sup> such as their excellent electrical performance,<sup>1</sup> high photo-thermal conversion efficiency,<sup>131,132</sup> and large specific surface area.<sup>125</sup> MXenes have fluorescence imaging properties and photo-thermal and antibacterial features, which are helpful in various biomedical applications.<sup>133</sup> This is due to the capability of MXene nanosheets to rapidly decompose upon interaction with water and oxygen. Consequently, it is possible to use these distinct photo-thermal characteristics and bio-based effectiveness for wound healing.<sup>134</sup> Many researchers have looked into the significance of MXenes in wound dressing applications. Some recent studies highlighted the importance of MXene-based composites for wound dressing applications. MXenes have anti-bacterial, photo-thermal, and luminescent attributes, making them suitable for a wide range of medical applications.<sup>135,136</sup> MXenes must be developed with various performance parameters without modifying their inherent properties to be used in medical applications. Notably, the influence of water and oxygen can deteriorate MXene nanosheets. Hence, employing these peculiar photo-thermal and bio-degradable activities for wound healing application is viable.<sup>137</sup>

MXenes have many elements, but titanium carbide ( $\text{Ti}_3\text{C}_2\text{T}_x$ ) is mainly used for wound healing. According to the reported studies, titanium shows the greatest potential in the biomedical

field given that it is an antimicrobial agent, shows cytotoxicity and has ROS (reactive oxygen species)-dependent characteristics, which ultimately enhance the cell viability.<sup>138</sup> ROS is essential in cell metabolic activities and viability and the anti-proliferative pathways of distinct classifications of carbon-based nanomaterials.<sup>139</sup> Hence,  $\text{Ti}_3\text{C}_2\text{T}_x$  MXenes are the most promising wound-healing materials given that they offer prospective benefits in the wound healing process through fibroblast proliferation. The increasing speed in wound repair is associated with previous wound contraction and stability of the impaired region reorganization of granulation tissue and collagen fibers.<sup>140</sup>

Lin Mao *et al.* (2020)<sup>141</sup> proposed that electrical stimulation can be applied to accelerate skin wound healing. However, electrical stimulation (ES) is rarely used to promote effective wound healing by encouraging skin cells behaviour. This study described the first sequence of multipurpose hydrogels made of regenerative  $\text{Ti}_3\text{C}_2\text{T}_x$  and bacterial cellulose (rBC), which can electrically control cell behaviour for effective wound repair with extrinsic ES. An amalgam hydrogel containing MXene of 2 wt% (rBC/MXene2%) had the optimum electrical conductivity, biocompatibility, mechanical characteristics, flexibility, and biodegradability. According to an *in vivo* investigation on a rat with a whole thickness damage specimen, this rBC/MXene hydrogel demonstrated superior healing effects compared to the conventional Tegaderm film. Mainly, the *in vivo* and *in vitro* findings showed that the hydrogel could remarkably boost NIH3T3 cell multiplication and speed up wound healing compared to the non-ES controls combined with ES. According to this report, the degradable and electro-active rBC/MXene hydrogel is a fascinating option for wound repairing on the skin. It also provides a successful synergistic treatment method for speeding wound healing by combining ES with hydrogel dressings. Fig. 5 represents the fabrication and synthesis of the rBC/MXene hydrogel.<sup>141</sup>

Similar research was done by Lin Jin *et al.* (2020),<sup>142</sup> wherein they proposed the synthesis of MXene nanobelts that respond to infrared light for wound healing applications. They offered temperature-responsive MXene nanobelt fibres (T-RMFs) with a controlled supply of vitamin E for wound healing applications. MXene nanosheets were dispersed over polyvinyl pyrrolidone and polyacrylonitrile composite nanobelts with a thermosensitive P(AAm-co-ANCO-VIm) (PAAV) coating layer to make these T-RMFs. The T-RMFs possessed outstanding photothermal characteristics because the MXene nanosheets had a high surface area and relatively high density. The temperature could be easily adjusted by NIR (near-infrared irradiation). The thermo-responsive polymer coating layer softened the bonds, allowing vitamin E to disintegrate and be released. The T-RMFs displayed remarkable bio-compatibility and wound healing activities in cellular and animal testing. These T-RMFs show that nanobelts have tremendous potential for wound healing, tissue regeneration, and a broad range of other applications. This is due to the simple technique, constant mass lifting, large surface area, outstanding wound curing activities, exciting nanosheet/nanobelt structure, enormous-scale productivity, and NIR-responsive features. This simple method for creating nanosheets and nanobelts opens up new possibilities for the





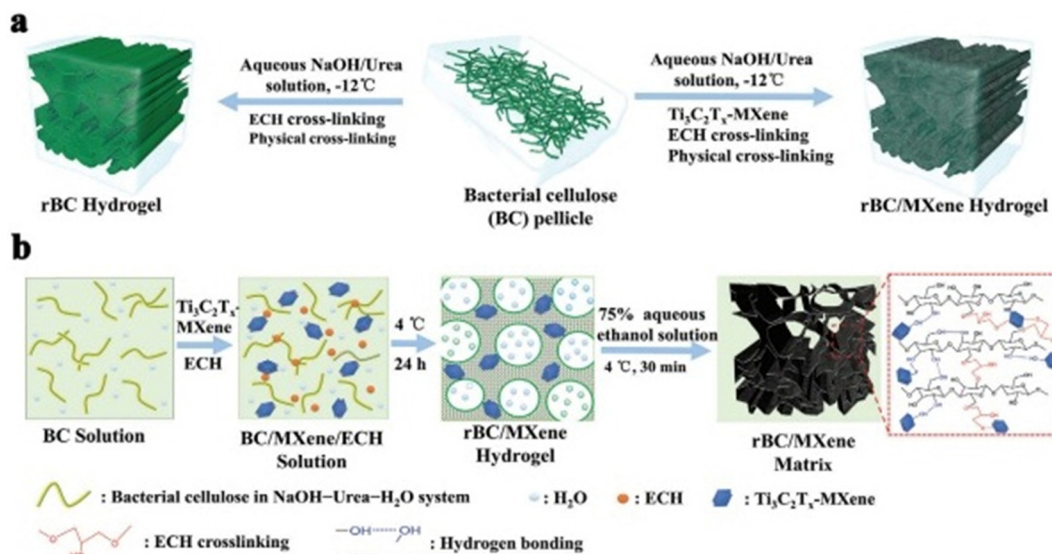


Fig. 5 (a) Schematic outlining the fabrication of rBC-based hydrogels. (b) Diagrammatic representation of the process for developing rBC/MXene composite hydrogels. (Adapted with permission from ref. 141 Copyright©2021.)

manufacturing and applications of nanomaterial. Fig. 6 describes the fabrication and coating of T-RMFs and Fig. 7 represents the healing of skin wounds with various groups.

Xu *et al.* (2021)<sup>38</sup> investigated a multimodal antimicrobial material based on an MXene to treat wound infections. They investigated electrostatic spinning nanofibrous membranes with a three-dimensional framework, which have been widely researched as potential wound-healing materials to preserve the water-absorbing balance in lesions and heal wounds. An MXene, polyvinyl alcohol (PVA), and amoxicillin

(AMX) were electrospun into an antimicrobial nanofibrous membrane (MXene-PVA-AMX nanofibrous-membrane). The PVA matrix in the nanocomposite membrane may stimulate the dissemination of AMX to fight against pathogens. Simultaneously, the MXene may convert near-infrared irradiation to heat, causing local hyperthermia and promoting the release of AMX. The bacteriostatic activity and wound healing capability of the composite nanofibrous membrane were tested *in vitro* on *S. aureus*- and *S. aureus*-infected mice as defected models. This film served as a physical block for loading the MXene

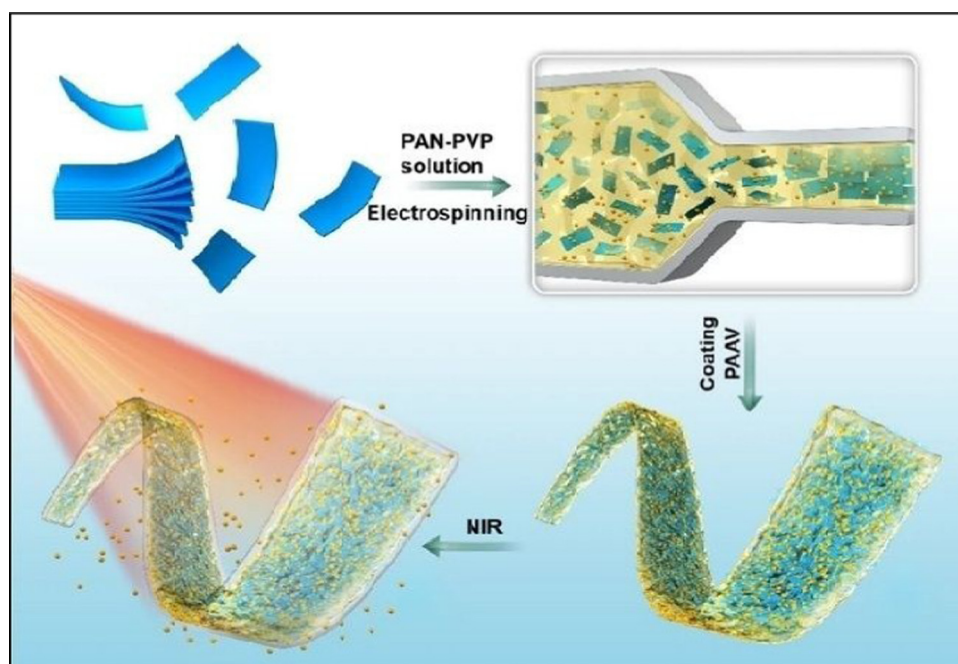


Fig. 6 Design of T-RMF nanobelt surface coating and fabrication (adapted from ref. 142 under Creative Commons License 4.0).



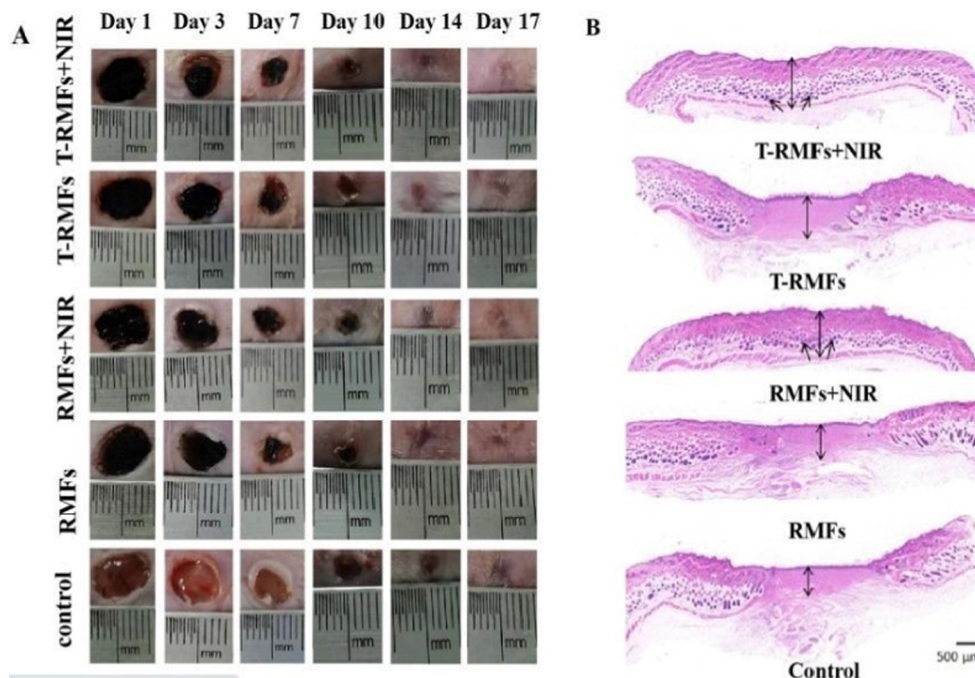


Fig. 7 Pictures of the skin wounds in different groups (T-RMF + NIR group, T-RMF group, RMF + NIR group, RMF group, and control group) on days 1, 3, 7, 10, 14, and 17 (adapted from ref. 142 under Creative Commons License 4.0).

and AMX. It demonstrated significant antimicrobial and rapid wound healing capabilities, paving the way for the development of new wound-healing dressings and antibacterial techniques.<sup>38</sup>

Interestingly, Mayerberger *et al.* (2018)<sup>143</sup> proposed the development of stretchable bandage composites with antibacterial properties by functionalizing electrospun CS nanofiber mats with  $\text{Ti}_3\text{C}_2\text{T}_z$  particles. Using an electrospinning method, they demonstrated how to develop embedded  $\text{Ti}_3\text{C}_2\text{T}_z$  (MXene) particles in chitosan nanofibers for inactive antimicrobial wound healing prospects.  $\text{Ti}_3\text{C}_2\text{T}_z$  particles were effectively integrated in the chitosan nanofibers without altering the strength of the nanofibers, as shown by SEM (Fig. 8(a) and

TEM Fig. 8(b)). The Gram -ve *E. coli* had a 95% reduction in colony-forming units, while the Gram +ve *S. aureus* had a 62% reduction in colony forming units after *in vitro* antibacterial investigations on crosslinked  $\text{Ti}_3\text{C}_2\text{T}_z$ /chitosan composite fibres. The bactericidal MXene/chitosan nanofibers were shown to be non-toxic after the cytotoxicity tests, proving their biocompatibility. The findings revealed that  $\text{Ti}_3\text{C}_2\text{T}_z$ /CS nanofiber mats have high antibacterial activity and may be effective wound dressing materials.<sup>143</sup>

Zhou *et al.* (2021)<sup>144</sup> created multi-functional scaffolds based on  $\text{Ti}_3\text{C}_2\text{T}_x$  MXene nanosheets, which exhibited an antibacterial hemostatic function for improving multidrug resistance bacteria-infected wound healing. In this study, a 2D (two-dimensional)

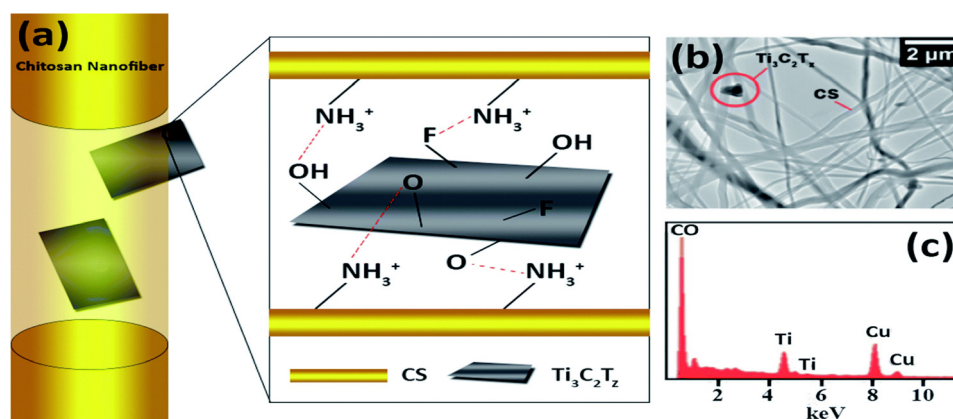


Fig. 8 (a) Schematic representations of the observed orientations of  $\text{Ti}_3\text{C}_2\text{T}_z$  flakes inside chitosan nanofibers. (b) Transmission electron microscopy image of the  $\text{Ti}_3\text{C}_2\text{T}_z$ /CS nano-fibers and (c) elemental examination (presence of copper is attributed to the TEM grid). (Adapted from ref. 143 under Creative Commons License 3.0, Copyright©2018, The Royal Society of Chemistry.)





$\text{Ti}_3\text{C}_2\text{T}_x\text{MXene}$  was employed to develop a multipurpose scaffold (HPEM) for wound healing with multidrug-resistant *Staphylococcus aureus* (MRSA). The HPEM scaffolds were created by combining poly(glycerol-ethylenimine),  $\text{Ti}_3\text{C}_2\text{T}_x\text{MXene}$ @polydopamine (MXene@PDA) nanosheets and oxidized hyaluronic acid (HCHO). Consequently, self-healing, electrical conductivity, tissue adhesion, antimicrobial activities, particularly for MRSA resistant to multiple commonly used medicines with 99.03% bactericidal effectiveness, and the ability to stop bleeding were all demonstrated in the HPEM scaffolds. Also, the HPEM scaffolds boosted natural skin cell proliferation, while offering low danger of damage.<sup>144</sup>

Moreover, the HPEM scaffolds stimulated the recovery of MRSA-infected wounds (ratio of wound closure of about 96.31%) by increasing collagen deposition, granulation tissue development, angiogenesis, vascular endothelial differentiation, and cell growth angiogenic process. This study demonstrated the usefulness of multi-functional 2D MXene@PDA nanosheets in the closure of infected wounds. MRSA-infected wounds and skin regeneration could be treated with the HPEM scaffolds with versatile characteristics. According to this study, multifunctional conductive HPEM scaffolds can expedite wound curing and skin repair by encouraging early

angiogenesis in infected wounds. Fig. 9 describes the healing of wounds infected by bacteria by using an HPEM scaffold.<sup>144</sup>

Sun *et al.* (2017)<sup>145</sup> prepared microneedle patches integrated with an MXene and encapsulated innate molecule for wound healing. A PBA (3-(acrylamido)phenylboronic acid) integrated with PEGDA (polyethylene glycol diacrylate) hydrogel was used as the host material of the microneedle patches (Fig. 10). This is because of the potential covalent interaction of boronate molecules with adenosine. The release of loaded adenosine may be enhanced under NIR irradiation due to the photo-thermal conversion capacity of the MXene to maintain the stimulation signal at the injury site. The MXene-integrated microneedle covered with encapsulated adenosine enhanced the angiogenesis *in vitro* cell studies. This study concluded that microneedle patches proliferated effectively when used to treat animal models.

Table 2 summarizes all the reported methods used for wound healing applications employing MXenes. This table overviews the work reported by various researchers.<sup>38,141–145</sup> Different raw materials such as regenerative bacterial cellulose (rBC),  $\text{Ti}_3\text{C}_2\text{T}_x$ , polyacrylonitrile, polyvinyl pyrrolidone composite nanobelts, amoxicillin (AMX), MXene, polyvinyl alcohol, CS nanofiber mats with  $\text{Ti}_3\text{C}_2\text{T}_x$  particles, poly(glycerol-ethylenimine),  $\text{Ti}_3\text{C}_2\text{T}_x\text{MXene}$ @polydopamine (MXene@PDA)

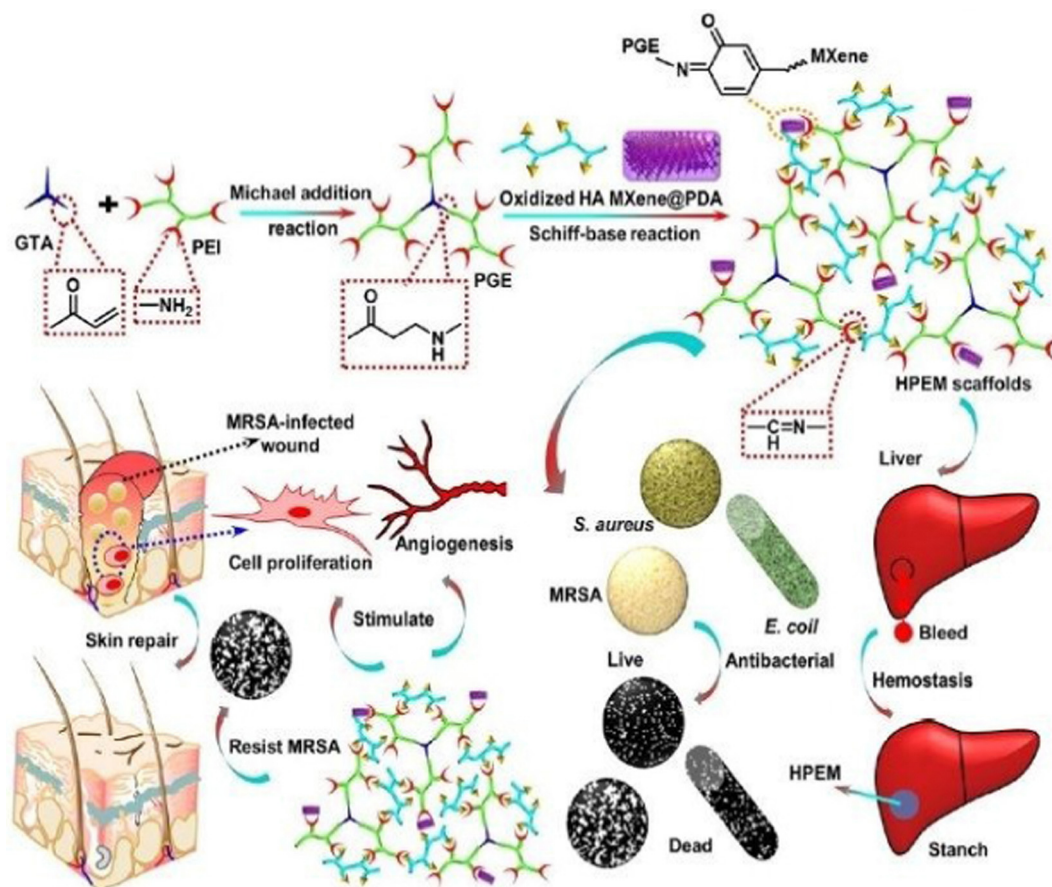


Fig. 9 Representation of the application and fabrication of HPEM scaffolds in multidrug-resistant bacteria-infected wound healing (adapted with permission from ref. 144 Copyright© 2021, the American Chemical Society).





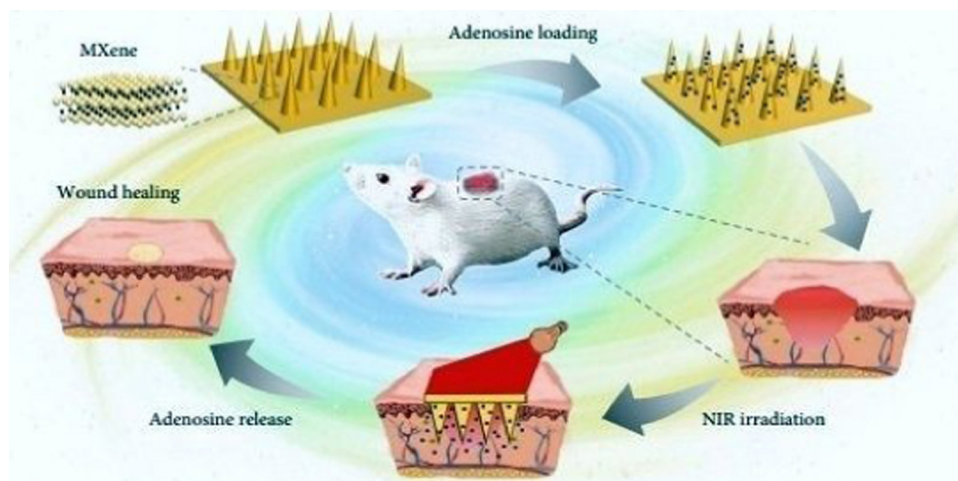


Fig. 10 Schematic illustration of the mechanism of MXene-integrated microneedle patches with the encapsulation of adenosine for healing wound. (Adapted from ref. 145 under Creative Commons License 4.0 Copyright © 2021.)

nanosheets, oxidized hyaluronic acid (HCHO), and PBA-(3-(acrylamido)phenyl boronic acid)-integrated PEGDA (polyethylene glycol diacrylate) hydrogel were used by various researchers. These materials were obtained as hydrogels, temperature-responsive MXene nanobelt fibres (T-RMFs), stretchable bandages, microneedle patches, nanofibrous membranes, *etc.* The main methods for the synthesis of these materials include electrical stimulation, electrospinning, and NIR irradiation for developing MXene-based materials for wound applications.

#### 4. Toxicity and biosafety issues

Due to its high efficiency, easy implementation and versatility in management, a wound treating method based on the conventional nature of the human skin has emerged in the last ten years and gained significant interest.<sup>146</sup> Conventional organic materials with superior cytocompatibility have been reported for various biological applications; however, their poor chemical/thermal stability and single capabilities are the main disadvantages impacting their progress in healthcare.<sup>147</sup> In contrast, inorganic 2D MXene-based nanomaterials have considerably large diagnostic interpretation prospects due to their intrinsic properties,<sup>148</sup> including easy bioconjugation, controllable morphological characteristics, favourable bio-compatibility, precise microbial degradation, multi-functionalism and comparatively high physiological consistency.<sup>149</sup> These characteristics are typically challenging to attain in most organic units. Even though MXenes have unique biomedicine practices, the bio-safety of the emerging 2D MXene family helps determine their ability in upcoming medical applications. In contrast to the well-researched carbon nanotubes, graphene oxide, and gold nano-systems, 2D MXenes and their compounds have recently become novel therapeutic nano-platforms. Consequently, investigation of their therapeutic and diagnostic effectiveness, biological impacts, and toxicology is still in its early stages.<sup>150</sup> The toxicity analysis of different 2D nanomaterials is under study; however, the medicinal chemistry effects of 2D nanomaterials,

such as their bioavailability, water-solubility, long-term toxic effects, and microbial degradation, remain unclear.<sup>25,151</sup>

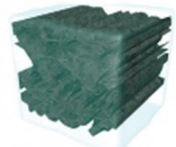
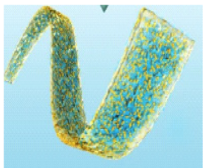
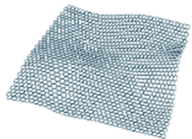

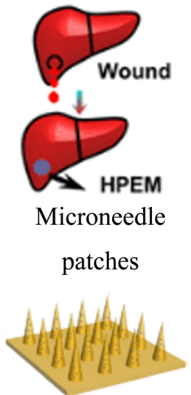
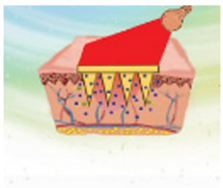
According to an investigation, MXenes and MXene-based composites have low cytotoxicity effects against cells. The probable bio-safety and bio-compatibility of surface-modified MXene nanosheets against mice were also assessed *in vivo*.<sup>152</sup> It was discovered that there was no difference in mouse behavior among the three treatment groups (exposed to NIR-I, NIR-II, and direct sunlight) and the control subjects. Also, no difference in mouse body weights was noticed over three durations. Haematoxylin and eosin (H&E) immune-histochemical assays were performed for significant organs (liver, heart, kidney, lung, and spleen) after a 28 day feed intake, with no apparent acute or chronic symptoms histopathologic toxic effects detected after comparison with the control and treatment groups. The blood tests were within normal parameters including haematological and cell biology factors. It is significant to note that Nb-based varieties produced by the bio-degradation of Nb<sub>2</sub>C MXene can foster the neogenesis and migration of blood vessels in the injured area, which can export more oxygen, vitamins, and energy around the surrounding bone during the repairment process, and also assemble more immune cells all over the damaged site to speed up the deterioration of the developed composite.<sup>153</sup> These findings suggest that Nb<sub>2</sub>C-PVP is bio-compatible for future *in vivo* tumour theranostic modalities. The same evaluations were performed on Ti<sub>3</sub>C<sub>2</sub> and Ta<sub>4</sub>C<sub>3</sub> MXenes<sup>134</sup> with marginal cytotoxic effects and sound *in vivo* biocompatibility. Moreover, regarding the present findings, more research and improvement of *in vitro* and *in vivo* toxicological evaluations, such as mutagenicity<sup>152</sup> and reproductive toxicity<sup>154</sup> are critical to fully utilize the ability of MXene-based theranostic nano-platforms for potent biomedical applications.

#### 5. Challenges and future outlook

Current research on MXenes and MXene-based materials emphasizes the significance of controlling their surface



Table 2 Summary of several types of MXenes for wound healing applications

S. no.	Raw materials	Method	MXene-based developed material	Ref.
			rBC/MXene Hydrogel	
1	Regenerative bacterial cellulose (rBC) and $\text{Ti}_3\text{C}_2\text{T}_x$	Electrical stimulation		141
			Temperature-responsive MXene nanobelt fibres (T-RMFs)	
2	Polyvinylpyrrolidone and polyacrylonitrile composite nanobelts with a thermosensitive coating layer of PAAV	NIR irradiation		142
			Nanofibrous membrane	
3	Amoxicillin (AMX), MXene, and polyvinyl alcohol (PVA)	Electro-spinning		38
			Stretchable bandage	
4	Electrospun CS nanofiber mats with $\text{Ti}_3\text{C}_2\text{T}_z$ particles	Electro-spinning		143
			Haemostatic multifunctional scaffold	
5	Poly(glycerol-ethylenimine), $\text{Ti}_3\text{C}_2\text{T}_x$ MXene@polydopamine (MXene@PDA) nanosheets, and oxidised hyaluronic acid (HCHO)	Fabrication and synthesis		144
6	PBA(3-(acrylamido)phenylboronic acid) integrated PEGDA (polyethylene glycol diacrylate) hydrogel	NIR irradiation		145



morphology for potentially innovative bioengineering and nanomedicine applications.<sup>155</sup> MXene-based nano-platforms must be biocompatible and stable in all physiological circumstances, with elevated targeting abilities, specificity and sustained release behavioral patterns.<sup>156</sup> MXenes have undoubtedly proven to possess numerous biological potencies, particularly in biological imaging, biosensors, cancer treatment, antimicrobial activities, drug tissue regeneration, and cell therapy, due to their unique physico-chemical characteristics.<sup>2,132</sup> These 2D materials can be efficiently designed and synthesized using cost-effective and straightforward techniques for complex healthcare gadgets.<sup>157</sup> By modifying their synthetic features and implementing optimum circumstances, their physical characteristics can be adjusted for particular uses such as wound dressings, power storage, imaging, biosensors, and water filtering. Also, MXenes have low toxicity and can be employed to treat cancer, germs and modulate the immune system.<sup>158</sup>

The marvellous electro-optic attributes of MXenes make them perfect representatives for detecting a broad spectrum of bio-electronic signals. Future studies should focus on functional scaffolds (both electrical and mechanical) for wound dressings, partition membranes for organ transplants, intracellular fluorescent probes and the transplantation of bio-electronic peripheral areas for identifying neuro-transmitter and bio-electronic signals. Furthermore, novel sustainability and eco-friendly synthetic approaches for the environmental-friendly

production of MXenes and their multifunctional modifications for novel wound dressing applications should be investigated.<sup>159</sup> The size and shape effects of MXenes on their characteristics and the interrelations between MXenes and drugs or cells must be thoroughly and technically evaluated. Also, their toxic effects, bio-compatibility, cytocompatibility, histological, and bio-safety concerns must also be systematically investigated, as shown in Fig. 11.

Bio-functionalization and biochemical surface changes can enhance numerous features, such as efficiency, durability, bio-availability, biocompatibility, and cytocompatibility, and minimize adverse effects/immune system responses and improve targeted properties.<sup>158,159,161</sup> Because of their high antibacterial action, the chemistry of MXenes enable their use in previously unexplored areas such as surface treatment of medical catheters, gloves, and masks.<sup>162</sup> However, research on bioactive MXene-based composites is still restricted. Greater emphasis should be paid to the systematic evaluation and modification of the cytotoxicity of MXene compounds.<sup>163,164</sup> The cell absorption characteristics, cytotoxic mechanisms, and *in vivo* and *in vitro* properties of MXenes, for example, should be thoroughly explored. Consequently, the physiological effects of MXenes must be entirely understood, given that MXene-based substances may accumulate in the body over time, potentially causing toxic effects. There have been no studies on the interactions of MXenes with the biological mechanism to date.<sup>46</sup>

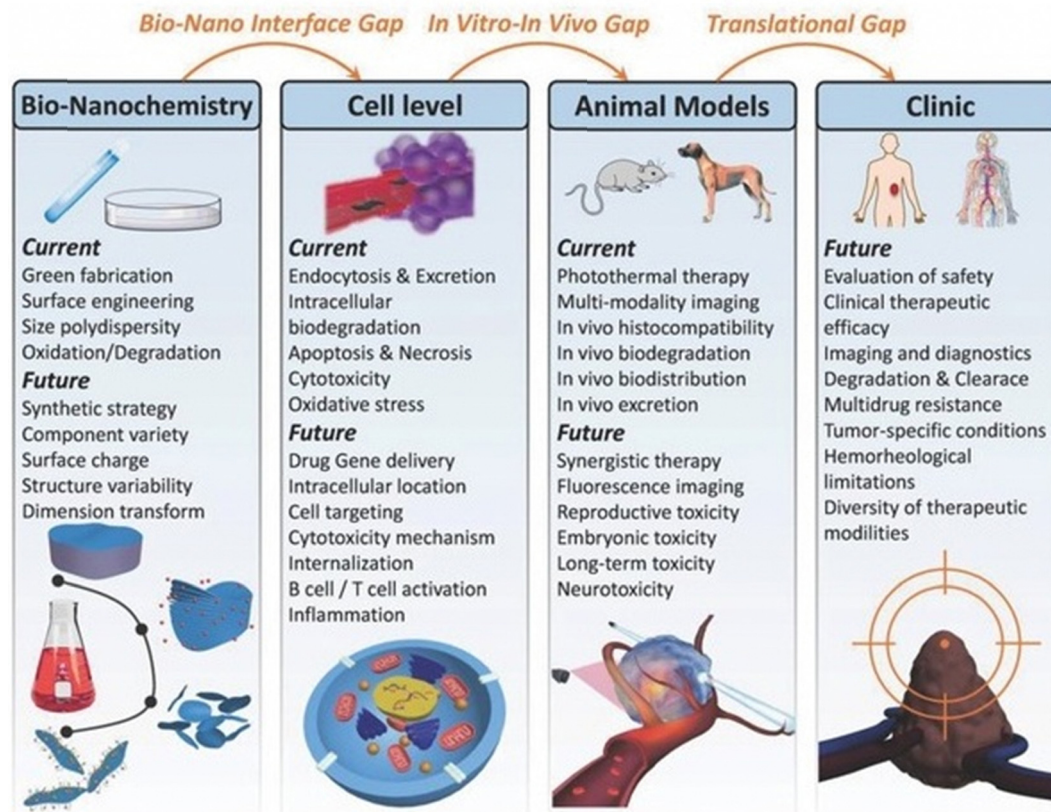


Fig. 11 Use of 2D ultrathin MXenes in the area of nanomedicine. (Adapted from ref. 160 under Creative Commons License 4.0 Copyright©2018.)





## 6. Conclusion

Due to their ultrathin structural features, unique morphological structures, and specialized physicochemical, electrical, optical, and biological properties, MXene-based materials have shown great potential in healthcare applications, particularly wound dressing applications. These materials can be fabricated using facile chemical processes such as electrical stimulation, electrospinning, and NIR irradiation to develop MXene-based materials, which can be helpful for applications in the healthcare sector. Further, the productivity of the samples can be improved by enhancing their chemical composition and the process parameters during their synthetic process. Especially for wound dressing applications, these MXene-based materials can be obtained in various forms such as hydrogen temperature-responsive MXene nanobelt fibres (TRMFs), stretchable bandages, microneedle patches, and nanofibrous membranes.

## Statement of ethical approval, ethical standards

The authors declare no involvement of animal studies or human participants in the study.

## Funding statement

This research received no specific grant from any funding agency.

## Conflicts of interest

The authors declare no conflict of interest.

## References

- 1 J. Li, H. Zhu, M. Zhang, X. Zheng, Z. Di, X. Liu and X. Wang, *Sci. Rep.*, 2014, **4**, 4359.
- 2 H. Huang, R. Jiang, Y. Feng, H. Ouyang, N. Zhou, X. Zhang and Y. Wei, *Nanoscale*, 2020, 1325–1338.
- 3 S. Verma, U. Dwivedi, K. Chaturvedi, N. Kumari, M. Dhangar, S. A. Hashmi, R. Singhal and A. K. Srivastava, *Synth. Met.*, 2022, **287**, 117095.
- 4 H. Riazi, K. Nemani, M. Grady, B. Anasori and M. Soroush, *J. Mater. Chem. A*, 2021, **9**, 8051–8098.
- 5 C. Zhang, L. Cui, S. Abdolhossein Zadeh and J. Heier, *InfoMat*, 2020, **4**, 613–638.
- 6 C. Peng, P. Wei, X. Chen, Y. Zhang, F. Zhu, Y. Cao, H. Wang, H. Yu and F. Peng, *Ceram. Int.*, 2018, **44**, 18886–18893.
- 7 H. Lin, S. Gao, C. Dai, Y. Chen and J. Shi, *J. Am. Chem. Soc.*, 2017, **139**, 16235–16247.
- 8 V. Shukla, *Mater. Adv.*, 2020, **9**, 3104–3121.
- 9 Z. Xiao, S. Ruan, L. B. Kong, W. Que, K. Zhou, Y. Liu and T. Zhang, *MXenes and MXenes-based Composites*, Springer Nature, 2020.
- 10 X. Zhan, C. Si, J. Zhou and Z. Sun, *Nanoscale Horizon.*, 2020, **5**, 235–258.
- 11 M. Mozafari and M. Soroush, *Mater. Adv.*, 2021, 7277–7307.
- 12 N. Baig and I. Kammakakam, *Mater. Adv.*, 2021, **2**, 1821–1871.
- 13 K. Hantanasirisakul, M. Q. Zhao, P. Urbankowski, J. Halim, B. Anasori, S. Kota, C. E. Ren, M. W. Barsoum and Y. Gogotsi, *Adv. Electron. Mater.*, 2016, **2**.
- 14 R. Sun, H. B. Zhang, J. Liu, X. Xie, R. Yang, Y. Li, S. Hong and Z. Z. Yu, *Adv. Funct. Mater.*, 2017, **27**, 1702807.
- 15 C. Ashley, E. Carnes, G. Phillips, D. Padilla, P. Durfee, P. Brown, T. Hanna, J. Liu, B. Phillips, M. Carter, N. Carroll, X. Jiang, D. Dunphy, C. Willman, D. Petsev, D. Evans, A. Parikh, B. Chackerian, W. Wharton and C. Brinker, *Naturematerials*, 2011, **10**, 476.
- 16 G. Hong, J. Lee, J. Robinson, U. Raaz, L. Xie, N. Huang, J. Cooke and H. Dai, *Nat. Med.*, 2012, **18**, 1841–1846.
- 17 N. Kotagiri, G. Sudlow, W. Akers and S. Achilefu, *Nat. Nanotechnol.*, 2015, **10**, 370–379.
- 18 S. Mura, J. Nicolas and P. Couvreur, *Nat. Mater.*, 2013, **12**, 991–1003.
- 19 H. Chen, W. Zhang, G. Zhu, J. Xie and X. Chen, *Nat. Rev. Mater.*, 2017, **2**, 17024.
- 20 M. Ferrari, *Nat. Rev. Cancer*, 2005, **5**, 161–171.
- 21 K. Shin, J. Choi, G. Ko, S. Baik, D. Kim, O. K. Park, K. Lee, H. R. Cho, S. Han, S. H. Lee, D. Lee, N. Lee, H. C. Kim and T. Hyeon, *Nat. Commun.*, 2017, **8**, 15807.
- 22 C. Liang, L. Xu, G. Song and Z. Liu, *Chem. Soc. Rev.*, 2016, **45**, 6250–6269.
- 23 Y. Lu, A. Aimetti, R. Langer and Z. Gu, *Nat. Rev. Mater.*, 2016, **1**, 16075.
- 24 D. Ni, W. Bu, E. Ehlerding, W. Cai and J. Shi, *Chem. Soc. Rev.*, 2017, **46**, 7438–7468.
- 25 H. Lin, Y. Chen and J. Shi, *Chem. Soc. Rev.*, 2018, **47**, 1938–1958.
- 26 K. Yang, L. Feng, X. Shi and Z. Liu, *Chem. Soc. Rev.*, 2012, **42**, 530–547.
- 27 G. Reina, J. González-Domínguez, A. CriadoFernández, E. Vázquez, A. Bianco and M. Prato, *Chem. Soc. Rev.*, 2017, **46**, 4400–4416.
- 28 X. Qian, Z. Gu and Y. Chen, *Mater. Horiz.*, 2017, **4**, 800–816.
- 29 H. Mao, S. Laurent, W. Chen, O. Akhavan, M. Imani, A. A. Ashkarran and M. Mahmoudi, *Chem. Rev.*, 2013, **113**, 3407–3424.
- 30 R. Kurapati, K. Kostarelos, M. Prato and A. Bianco, *Adv. Mater.*, 2016, **28**, 6052–6074.
- 31 L. Feng, L. Wu and X. Qu, *Adv. Mater.*, 2013, **25**, 168–186.
- 32 D. Chimene, D. Alge and A. Gaharwar, *Adv. Mater.*, 2015, **27**, 7261–7284.
- 33 Y. Chen, C. L. Tan and H. Zhang, *Catal. Commun.*, 2015, **44**, 2681–2701.
- 34 A. Naskar and K. Kim, *Pharmaceutics*, 2020, **12**, 499.
- 35 S. Dhivya, V. Padma and S. Elango, *BioMedicine*, 2015, **5**, 1–5.
- 36 S. Baranoski and E. Ayello, *Adv. Skin Wound Care*, 2012, **25**, 87–92; quiz 92.
- 37 D. Simões, S. Miguel, M. Ribeiro, P. Coutinho, A. Mendonça and I. Correia, *Eur. J. Pharm. Biopharm.*, 2018, **127**, 130–141.



- 38 X. Xu, S. Wang, H. Wu, Y. Liu, F. Xu and J. Zhao, *Colloids Surf., B*, 2021, **207**, 111979.
- 39 R. Ronchi, J. Arantes and S. Santos, *Ceram. Int.*, 2019, **45**, 18167–18188.
- 40 L. Fu, *Adv. Eng. Mater.*, 2020, **23**, 2001191.
- 41 P. Eklund, M. Beckers, U. Jansson, H. Högberg and L. Hultman, *Thin Solid Films*, 2010, **518**, 1851–1878.
- 42 M. Barsoum and P. Eklund, *The  $M_{n+1}AX_n$  Phases: The Precursors for MXenes*, 2019, pp. 15–35.
- 43 M. Barsoum, *A New Class of Solids; Thermodynamically Stable Nanolaminates*, 2000, vol. 28, pp. 28–201.
- 44 M. Barsoum, *MAX Phases: Properties of Machinable Ternary Carbides and Nitrides*, 2013.
- 45 I. Low, *Advances in Science & Technology of MAX Phases*, 2012.
- 46 A. Zamhuri, G. Lim, N. L. Ma, K. Tee and C. Soon, *BioMed. Eng. OnLine*, 2021, **20**, 1–24.
- 47 M. Naguib, V. Mochalin, M. Barsoum and Y. Gogotsi, *Adv. Mater.*, 2014, **26**, 982.
- 48 M. Khazaei, M. Arai, T. Sasaki, C.-Y. Chung, V. Natarajan Sathiyamoorthy, M. Estili, Y. Sakka and Y. Kawazoe, *Adv. Funct. Mater.*, 2013, **23**, 2185–2192.
- 49 J. Zhou, X.-H. Zha, Z. Xiaobing, F. Chen, G. Gao, S. Wang, C. Shen, T. Chen, C. Zhi, P. Eklund, S. Du, J. Xue, W. Shi, Z. Chai and Q. Huang, *ACS Nano*, 2017, **11**, 3841–3850.
- 50 A. Enyashin and A. Ivanovskii, *J. Solid State Chem.*, 2013, **207**, 42–48.
- 51 N. Chaudhari, H. Jin, B. Kim, D. S. Baek, S. Joo and K. Lee, *J. Mater. Chem. A*, 2018, **6**, 24564–24579.
- 52 M. Naguib, O. Mashtalir, J. Carle, V. Presser, J. Lu, L. Hultman, Y. Gogotsi and M. Barsoum, *ACS Nano*, 2012, **6**, 1322–1331.
- 53 K. Papadopolou, A. Chroneos, D. Parfitt and S.-R. G. Christopoulos, *J. Appl. Phys.*, 2020, **128**, 170902.
- 54 M. Naguib, M. Kurtoglu, V. Presser, J. Lu, J. Niu, M. Heon, L. Hultman, Y. Gogotsi and M. Barsoum, *Adv. Mater.*, 2011, **23**, 4207.
- 55 J. Halim, M. Lukatskaya, K. Cook, J. Lu, C. Smith, L.-Å. Näslund, S. May, L. Hultman, Y. Gogotsi, P. Eklund and M. Barsoum, *Chem. Mater.*, 2014, **26**, 2374–2381.
- 56 J. Pang, R. Mendes, A. Bachmatiuk, L. Zhao, H. Ta, T. Gemming, H. Liu, Z. Liu and M. Rummeli, *Chem. Soc. Rev.*, 2018, **48**, 72–133.
- 57 B. Wyatt, A. Rosenkranz and B. Anasori, *Adv. Mater.*, 2021, **33**, 2007973.
- 58 L. Verger, V. Natu, M. Carey and M. Barsoum, *Trends Chem.*, 2019, **1**, 656–669.
- 59 J. Zhou, S. Gao, Z. Guo and Z. Sun, *Ceram. Int.*, 2017, **43**, 11450–11454.
- 60 M. Tran, T. Schäfer, A. Shahraei, M. Duerrschabel, L. Molina-Luna, U. Kramm and C. Birkel, *ACS Appl. Energy Mater.*, 2018, **1**, 3908–3914.
- 61 M. Ghidui, M. Lukatskaya, M.-Q. Zhao, Y. Gogotsi and M. Barsoum, *Nature*, 2014, 78–81.
- 62 J. Yang, W. Bao, P. Jaumaux, S. Zhang, C. Wang and G. Wang, *Adv. Mater. Interfaces*, 2019, **6**, 1802004.
- 63 Y. Gogotsi, *Nat. Mater.*, 2015, **14**, 1079–1080.
- 64 L. Ma, L. Ting, V. Molinari, C. Giordano and B. Yeo, *J. Mater. Chem. A*, 2015, **3**, 8361–8368.
- 65 T. Li, L. Yao, Q. Liu, J. Gu, R. Luo, J. Li, X. Yan, W. Wang, P. Liu and B. Chen, *Angew. Chem., Int. Ed.*, 2018, **57**, 6115–6119.
- 66 S. Yang, P. Zhang, F. Wang, A. G. Ricciardulli, M. Lohe, P. Blom and X. Feng, *Angew. Chem., Int. Ed.*, 2018, **57**, 15491–15495.
- 67 W. Sun, S. Shah, Y. Chen, Z. Tan, H. Gao, T. Habib, M. Radovic and M. Green, *J. Mater. Chem. A*, 2017, **5**, 21663–21668.
- 68 P. Urbankowski, B. Anasori, T. Makaryan, D. Er, S. Kota, P. Walsh, M. Zhao, V. Shenoy, M. Barsoum and Y. Gogotsi, *Nanoscale*, 2016, **8**, 11385–11391.
- 69 L. Verger, C. Xu, V. Natu, H. M. Cheng, W. Ren and M. Barsoum, *Curr. Opin. Solid State Mater. Sci.*, 2019, **23**, 149–163.
- 70 L. Karlsson, J. Birch, J. Halim, M. Barsoum and P. Persson, *Nano Lett.*, 2015, **15**, 4955–4960.
- 71 M. Li, J. Lu, K. Luo, Y. Li, K. Chang, K. Chen, J. Zhou, J. Rosén, L. Hultman, P. Eklund, P. Persson, S. Du, Z. Chai, Z. Huang and Q. Huang, *Element Replacement Approach by Reaction with Lewis Acidic Molten Salts to Synthesize Nanolaminated MAX Phases and MXenes*, 2019.
- 72 A. Sundaram, J. Ponraj, C. Wang, W. K. Peng, M. Kumar, S. Dhanabalan and J. Gaspar, *J. Mater. Chem. B*, 2020, **8**, 4990–5013.
- 73 H. Huang, W. Feng, Y. Chen and J. Shi, *Nano Today*, 2020, **35**, 100972.
- 74 S. Wang, H. Zheng, L. Zhou, F. Cheng, C. K. Liu, H. Zhang, L. Wang and Q. Zhang, *Nano Lett.*, 2020, 5149–5158.
- 75 K. Huang, Z. Li, J. Lin, G. Han and P. Huang, *Chem. Soc. Rev.*, 2018, **47**, 5109–5124.
- 76 J. Heikenfeld, A. Jajack, J. Rogers, P. Gutruf, L. Tian, T. Pan, R. Li, M. Khine, J. Kim and J. Wang, *Lab Chip*, 2018, **2**, 217–248.
- 77 Y. Liu, M. Pharr and G. A. Salvatore, *ACS Nano*, 2017, **10**, 9614–9635.
- 78 F. Vitale and B. Litt, *Bioelectron. Med.*, 2018, **1**, 3–7.
- 79 J. J. Norton, D. S. Lee, J. W. Lee, W. Lee, O. Kwon, P. Won, S. Y. Jung, H. Cheng, J. W. Jeong, A. Akce and S. Umunna, *Proc. Natl. Acad. Sci. U. S. A.*, 2015, **13**, 3920–3925.
- 80 B. Xu, A. Akhtar, Y. Liu, H. Chen, W. H. Yeo, S. I. Park, B. Boyce, H. Kim, J. Yu, H. Y. Lai and S. Jung, *Adv. Mater.*, 2016, **22**, 4462–4471.
- 81 D. McFarland and J. R. Wolpaw, *Curr. Opin. Biomed. Eng.*, 2017, **4**, 194–200.
- 82 S. Lee, W. Y. Peh, J. Wang, F. Yang, J. S. Ho, N. V. Thakor, S. C. Yen and C. Lee, *Adv. Sci.*, 2017, **11**, 1700149.
- 83 M. R. DeLong and T. Wichmann, *JAMA Neurol.*, 2015, **11**, 1354–1360.
- 84 G. T. Hwang, H. Park, J. H. Lee, S. Oh, K. I. Park, M. Byun, H. Park, G. Ahn, C. K. Jeong, K. No and H. Kwon, *Adv. Mater.*, 2014, **28**, 4754.
- 85 L. Ulloa, S. Quiroz-Gonzalez and R. Torres-Rosas, *Trends Mol. Med.*, 2017, **12**, 1103–1120.



- 86 J. Cheng, H. Shen, R. Chowdhury, T. Abdi, F. Selaru and J. D. Chen, *Inflamm. Bowel Dis.*, 2020, **8**, 1119–1130.
- 87 N. Driscoll, B. Erickson, B. B. Murphy, A. G. Richardson, G. Robbins, N. V. Apollo, G. Mentzelopoulos, T. Mathis, K. Hantanasirisakul, P. Bagga and S. E. Gullbrand, *Sci. Transl. Med.*, 2021, **612**, eabf8629.
- 88 Y. Bai, K. Zhou, S. Narasimalu, J. Pang, X. He and R. Wang, *RSC Adv.*, 2016, **6**, 35731–35739.
- 89 M. Magnuson, J. Halim and L.-Å. Näslund, *J. Electron Spectrosc. Relat. Phenom.*, 2018, **224**, 27–32.
- 90 X.-H. Zha, J. Yin, Y. Zhou, Q. Huang, K. Luo, J. Lang, J. Francisco, J. He and S. Du, *J. Phys. Chem. C*, 2016, **120**, 15082–15088.
- 91 P. Chakraborty, T. Das, D. Nafday, L. Boeri and T. Saha-Dasgupta, *Phys. Rev. B*, 2017, **95**, 184106.
- 92 U. Yorulmaz, A. Ozden, N. Perkgoz, F. Ay and C. Sevik, *Nanotechnology*, 2016, **27**, 335702.
- 93 O. Mashtalir, M. Lukatskaya, A. Kolesnikov, E. Raymundo-Piñero, M. Naguib, M. Barsoumand and Y. Gogotsi, *Nanoscale*, 2016, **8**, 9128–9133.
- 94 B. Anasori, M. R. Lukatskaya and Y. Gogotsi, *Nat. Rev. Mater.*, 2017, **2**, 1–17.
- 95 V. Borysiuk, V. Mochalin and Y. Gogotsi, *Nanotechnology*, 2015, **26**, 265705.
- 96 V. Borysiuk and V. Mochalin, *MRS Commun.*, 2019, **9**, 1–6.
- 97 C. Zhang and V. Nicolosi, *Energy Storage Mater.*, 2018, **16**, 102–125.
- 98 A. Ivanovskii and A. Enyashin, *Russian Chem. Rev.*, 2013, **82**, 735.
- 99 K. Hantanasirisakul and Y. Gogotsi, *Adv. Mater.*, 2018, **30**, 1804779.
- 100 H. Kim, Z. Wang and H. Alshareef, *Nano Energy*, 2019, **60**, 179–197.
- 101 L. Dong, H. Kumar, B. Anasori, Y. Gogotsi and V. Shenoy, *J. Phys. Chem. Lett.*, 2016, **8**, 422–428.
- 102 B. Anasori, Y. Xie, M. Beidaghi, J. Lu, B. Hosler, L. Hultman, P. Kent, Y. Gogotsi and M. Barsoum, *ACS Nano*, 2015, **9**, 9507–9516.
- 103 B. Anasori, C. Shi, E. J. Moon, Y. Xie, C. Voigt, P. Kent, S. May, S. Billinge, M. Barsoum and Y. Gogotsi, *Nanoscale Horiz.*, 2016, **1**, 227–234.
- 104 W. Sun, Y. Xie and P. Kent, *Nanoscale*, 2018, **10**, 11962–11968.
- 105 Q. Tao, M. Dahlqvist, J. Lu, S. Kota, R. Meshkian, J. Halim, J. Palisaitis, L. Hultman, M. Barsoum, P. Persson and J. Rosén, *Nat. Commun.*, 2017, **8**, 14949.
- 106 M. Dahlqvist, A. Petruhins, J. Lu, L. Hultman and J. Rosen, *ACS Nano*, 2018, **12**, 7761–7770.
- 107 J. Zhu, A. Chroneos, J. Eppinger and U. Schwingenschlögl, *Appl. Mater. Today*, 2016, **5**, 19–24.
- 108 A. Bandyopadhyay, D. Ghosh and S. Pati, *Phys. Chem. Chem. Phys.*, 2018, **20**, 4012–4019.
- 109 K. Chaudhuri, Z. Wang, M. Alhabeb, K. Maleski, Y. Gogotsi, V. Shalaev and A. Boltasseva, *Optical properties of MXenes*, 2019, pp. 327–346.
- 110 J. Halim, I. Persson, E. Moon, P. Kühne, V. Darakchieva, P. Persson, P. Eklund, J. Rosén and M. Barsoum, *J. Phys.: Condens. Matter*, 2019, **31**, 165301.
- 111 X. Jiang, S. Liu, W. Liang, C. S. Luo, Z. He, Y. Ge, H. Wang, R. Cao, F. Zhang, Q. Wen, J. Li, Q. Bao and D. Fan, *Laser Photonics Rev.*, 2018, **12**, 1700229.
- 112 X. Jiang, A. Kuklin, A. Baev, Y. Ge, H. Agren and P. Prasad, *Phys. Rep.*, 2020, 1–58.
- 113 O. Akhavan and E. Ghaderi, *ACS Nano*, 2010, **4**, 5731–5736.
- 114 S. Chernousova and M. Epple, *Angew. Chem., Int. Ed.*, 2012, **52**, 1636–1653.
- 115 J. Lemire, J. Harrison and R. Turner, *Nat. Views, Microbiol.*, 2013, **11**, 371–384.
- 116 Y. Li, W. Zhang, J. Niu and Y. Chen, *ACS Nano*, 2012, **6**, 5164–5173.
- 117 K. Rasool, M. IHelal, A. Ali, C. Ren, Y. Gogotsi and K. Mahmoud, *ACS Nano*, 2016, **10**, 3674–3684.
- 118 K. Rasool, K. Mahmoud, D. Johnson, M. IHelal, G. Berdiyrov and Y. Gogotsi, *Sci. Rep.*, 2017, **7**, 1598.
- 119 A. Shamsabadi, G. H. Sharifian, B. Anasori and M. Soroush, *ACS Sustainable Chem. Eng.*, 2018, **6**, 16586–16596.
- 120 G. Lim, C. Soon, M. Morsin, M. K. Ahmad, N. Nayan and K. Tee, *Ceram. Int.*, 2020, **46**, 20306–20312.
- 121 S. Mahmoudi, E. Mancini, L. Xu, A. Moore, F. Jahanbani, K. Hebestreit, R. Srinivasan, X. Li, K. Devarajan, L. Prélôt, C. E. Ang, Y. Shibuya, B. Benayoun, A. Chang, M. Wernig, J. Wysocka, M. Longaker, M. Snyder and A. Brunet, *Nature*, 2019, **574**, 553–558.
- 122 R. Tetley, M. Staddon, S. Banerjee and Y. Mao, *Tissue Fluid. Promotes Epithelial Wound Heal.*, 2018, 1195–1203.
- 123 X. Zhao, A. Vashisth, J. Blivin, Z. Tan, D. Holta, V. Kotasthane, S. Shah, T. Habib, S. Liu, J. Lutkenhaus, M. Radovic and M. Green, *Adv. Mater. Interfaces*, 2020, **7**, 2000845.
- 124 R. Hou, L. Wu, J. Wang, Z. Yang, Q. Tu and N. Huang, *Biomolecules*, 2019, **9**, 69.
- 125 X. Wang, J. Jin, R. Hou, M. Zhou, X. Mou, K. Xu, Y. Zhu, Z. Shen and X. Zhang, *ACS Appl. BioMater.*, 2019, 735–746.
- 126 J. Ouyang, X. Ji, X. Zhang, C. Feng, Z. Tang, N. Kong, A. Xie, A. Wang, X. Sui, L. Deng, Y. Liu, J. Kim, Y. Cao and W. Tao, *Proc. Natl. Acad. Sci. U. S. A.*, 2020, **117**, 28667–28677.
- 127 T. Cui, J. Yu, Q. Li, C.-F. Wang, S. Chen, W. Li and G. Wang, *Adv. Mater.*, 2020, **32**, 2000982.
- 128 W. Srifa, N. Kosaric, A. Amorin, O. Jadi, Y. Park, S. Mantri, J. Camarena, G. Gurtner and M. Porteus, *Nat. Commun.*, 2020, **11**, 1–4.
- 129 Z.-K. Li, Y. Wei, X. Gao, L. Ding, Z. Lu, J. Deng, X. Yang, J. Caro and H. Wang, *Angew. Chem., Int. Ed.*, 2020, **59**, 9838–9843.
- 130 D. Xu, Z. Li, L. Li and J. Wang, *Adv. Funct. Mater.*, 2020, **30**, 2000712.
- 131 J. Lao, S. Wu, J. Gao, A. Dong, G. Li and J. Luo, *Nano Energy*, 2020, **70**, 104481.
- 132 Q. Gao and H. Zhang, *Nanoscale*, 2020, **12**, 5995–6001.
- 133 S. Pan, J. Yin, L. Yu, C. Zhang, Y. Zhu, Y. Gao and Y. Chen, *Adv. Sci.*, 2020, **7**, 1901511.
- 134 X. Lin, Z. Li, J. Qiu, Q. Wang, J. Wang and T. Chen, *Biomater. Sci.*, 2021, **9**, 5437–5471.
- 135 D. Gao, X. Guo, X. Zhang, S. Chen, Y. Wang, T. Chen, G. Huang, Y. Gao, Z. Tian and Z. Yang, *Mater. Today Bio*, 2020, **5**, 100035.





- 136 S. Pan, J. Yin, L. Yu, C. Zhang, Y. Zhu, Y. Gao and Y. Chen, *Adv. Sci.*, 2020, **2**, 1901511.
- 137 H. Liao, X. L. Guo, P. B. Wan and G. H. Yu, *Adv. Funct. Mater.*, 2019, **29**, 19040507.
- 138 A. Nikpasand and M. R. Parvizi, *Bull. Emerg. Trauma*, 2019, **4**, 366.
- 139 A. M. Jastrzębska, A. Szuplewska, T. Wojciechowski, M. Chudy, W. Ziemkowska, L. Chlubny, A. Rozmysłowska and A. Olszyna, *J. Hazardous Mater.*, 2017, **339**, 1–8.
- 140 A. J. Alanis, *Arch. Med. Res.*, 2005, **36**, 697–705.
- 141 L. Mao, S. Hu, Y. Gao, L. Wang, W. Zhao, L. Fu, H. Cheng, L. Xia, S. Xie, W. Ye, Z. Shi and G. Yang, *Adv. Healthcare Mater.*, 2020, 2000872.
- 142 L. Jin, X. Guo, D. Gao, C. Wu, B. Hu, G. Tan, N. Du, X. Cai and Z. Yang, *NPG Asia Mater.*, 2021, **13**, 1–9.
- 143 E. Mayerberger, R. Street, R. McDaniel, M. Barsoum and C. Schauer, *RSC Adv.*, 2018, **8**, 35386–35394.
- 144 L. Zhou, H. Zheng, Z. Liu, S. Wang, C. K. Liu, F. Chen, H. Zhang, J. Kong, F. Zhou and Q. Zhang, *ACS Nano*, 2021, **15**, 2468–2480.
- 145 L. Sun, L. Fan, F. Bian, G. Chen, Y. Wang and Y. Zhao, *Research*, 2021, 1–9.
- 146 R. Yu, H. Zhang and B. Guo, *Nano-Micro Lett.*, 2022, **1**, 1–46.
- 147 Y. Niu, J. Li, J. Gao, X. Ouyang, L. Cai and Q. Xu, *Nano Res.*, 2021, **11**, 3820–3839.
- 148 K. Khan, A. K. Tareen, M. Aslam, R. U. Sagar, B. Zhang, W. Huang, A. Mahmood, N. Mahmood, K. Khan, H. Zhang and Z. Guo, *Nano-Micro Lett.*, 2020, **1**, 1–77.
- 149 S. Song, X. Jiang, H. Shen, W. Wu, Q. Shi, M. Wan, J. Zhang, H. Mo and J. Shen, *ACS Appl. BioMater.*, 2021, **4**, 6912–6923.
- 150 L. Zong, H. Wu, H. Lin and Y. Chen, *Nano Res.*, 2018, **8**, 4149–4168.
- 151 X. Zhang, L. Cheng, Y. Lu, J. Tang, Q. Lv, X. Chen, Y. Chen and J. Liu, *Nano-Micro Lett.*, 2022, **1**, 1–21.
- 152 O. Akhavan, E. Ghaderi and A. Akhavan, *Biomaterials*, 2012, **33**, 8017–8025.
- 153 J. Yin, S. Pan, X. Guo, Y. Gao, D. Zhu, Q. Yang, J. Gao, C. Zhang and Y. Chen, *Nano-Micro Lett.*, 2021, **1**, 1–8.
- 154 O. Akhavan, *Carbon*, 2015, **81**, 158–166.
- 155 A. Rozmysłowska-Wojciechowska, J. Mitrzak, A. Szuplewska, M. Chudy, J. Woźniak, M. Petrus, T. Wojciechowski, A. Vasilchenko and A. Jastrzębska, *Materials*, 2020, **13**, 17.
- 156 M. Xin, J. Li, Z. Ma, L. Pan and Y. Shi, *Front. Chem.*, 2020, **8**, 297.
- 157 G. JamalipourSoufi and S. Irvani, *Green Chem.*, 2020, **22**, 2662–2687.
- 158 S. Irvani and R. Varma, *Environ. Chem. Lett.*, 2020, **18**, 703–727.
- 159 S. Irvani and R. Varma, *Mater. Adv.*, 2021, 2906–2917.
- 160 H. Lin, Y. Hen and J. Shi, *Adv. Sci.*, 2018, **5**, 1800518.
- 161 G. JamalipourSoufi, P. Irvani, A. Hekmatnia, E. Mostafavi, M. Khatami and S. Irvani, *Comments on Inorganic Chemistry*, 2021, pp. 1–34.
- 162 L. Wang, P. Hu, Z. Liu and X. He, *J. Mater. Chem. A*, 2017, **5**, 22855–22876.
- 163 A. Zavabeti, A. Jannat, L. Zhong, A. Haidry, Z. Yao and J. Ou, *Nano-Micro Lett.*, 2020, **12**, 1–34.
- 164 B. Lu, Z. Zhu, B. Ma, W. Wang, R. Zhu and J. Zhang, *Small*, 2021, 2100946.

